Research Square

Preprints are preliminary reports that have not undergone peer review.
They should not be considered conclusive, used to inform clinical practice,
or referenced by the media as validated information.

Effect of Lightweight Design on Structural Dynamics and Energy Efficiency in Hydraulically Actuated Flexible Systems

Tirtha Gupta

tirtha.gupta@oulu.fi

University of Oulu

Aleksi Härkönen

Lappeenranta University of Technology

Dominik Walica

University of Oulu

Qasim Khadim

University of Oulu

Antti Ahola

Lappeenranta University of Technology

Emil Kurvinen

University of Oulu

Method Article

Keywords: Lightweight Structures, Flexible Multibody Systems, Finite Element Analysis, Hydraulics

Posted Date: June 12th, 2025

DOI: https://doi.org/10.21203/rs.3.rs-6567260/v1

License: This work is licensed under a Creative Commons Attribution 4.0 International License.
Read Full License

Additional Declarations: No competing interests reported.

Effect of Lightweight Design on Structural Dynamics and Energy Efficiency in Hydraulically Actuated Flexible Systems

Tirtha Gupta*[,1], Aleksi Härkönen[2], Dominik Walica[1], Qasim Khadim[1], Antti Ahola[2], Emil Kurvinen[1]

[1]Materials and Mechanical Engineering, University of Oulu, Pentti Kaiteran katu 1, Oulu, 90570, Finland.
[2]Steel Structures, LUT University, Yliopistonkatu 34, Lappeenranta, 53850, Finland.
*Corresponding author, email: tirtha.gupta@oulu.fi.

Abstract

Growing demands for environmental sustainability, energy efficiency, and enhanced automation are reshaping the design of heavy machinery, particularly hydraulic systems. This study introduces a workflow for the lightweight and energy efficient design of hydraulically actuated flexible multibody systems. The component of interest, lift boom was manufactured from RAEX 640 steel, was optimized using Ultra-High Strength Steel (UHSS). The structural characteristics of default and optimized lift boom were compared through linear structural analysis, and the impact on the system's energy efficiency was evaluated through a simulated work cycle. This optimization achieved a 21.9% reduction in weight when only in-plane moment capacity was considered. However, the reduced cross-sectional geometry, resulted in a 67% increase in tip deflection and eigenfrequency analysis revealed a shift of the critical first bending mode frequency from 104.6 Hz to 67.5 Hz. Flexible multibody dynamic simulations, including hydraulic actuation modeling, confirmed improved energy efficiency by 4% during an extension and by 7% during retraction phase. While the weight reduction benefits were clear, the findings underscore the importance of carefully balancing weight savings with mechanical performance criteria to ensure safe and efficient operation. The proposed workflow not only addresses current challenges in lightweight design for hydraulically actuated systems but also establishes a foundation for real-time digital twin development, supporting the evolution of smart, energy-efficient heavy machinery.

Keywords: Lightweight Structures, Flexible Multibody Systems, Finite Element Analysis, Hydraulics.

1 Introduction

Growing environmental concerns, including emissions produced by heavy machinery [1, 2] are reshaping design requirements and driving the need for safer, more energy-efficient operations. Heavy machinery, typically hydraulically actuated and often operated manually, plays a key role in material handling and construction activities. Emerging trends of automation, electrification, and higher productivity are pushing engineers to design lightweight machines, creating challenges in design, material selection and manufacturing [3, 4]. Lightweighting, achieved by optimizing components to reduce structural mass without compromising performance, has become a key strategy to meet these demands.

Reducing structural mass, however, inherently involves trade-offs between mechanical properties (e.g., stiffness, deformation, and fatigue resistance), overall system performance, manufacturing complexity, and environmental impacts across the product life cycle [5]. To manage some of these trade-offs, design optimization methods focus on minimizing weight while ensuring that functionality and structural strength remain within acceptable limits [6]. Material selection, geometric refinement, and shape optimization are crucial tools in this process [7]. To support early-stage decision-making and evaluate complex interactions between performance targets, engineers increasingly rely on virtual prototyping tools.

Several approaches have been proposed to apply lightweighting strategies to hydraulically actuated systems. For instance, Zhang et al. [8] optimized an excavator lift boom structure using a surrogate model, achieving a 9.3% weight reduction compared to the original design, despite a 5.09% increase in maximum stress and an 8.27% increase in deformation, while still meeting fatigue design requirements. However, the impact of lightweighting on the structure's dynamic behavior was not investigated. Similarly, Solazzi et al. [9] redesigned excavator arms using unconventional composite materials, reporting a 64.1% weight reduction, but their evaluation was limited to low-frequency loading cycles, without fully assessing structural dynamics under operational conditions.

Structural dynamic performance is a critical factor when evaluating overall machine behavior under real working conditions. Lightweighting affects not only static properties but also system dynamics, energy efficiency, and control performance [10–12]. While some studies mention a potential positive impact of lightweighting on machine characteristics, comprehensive evaluations of dynamic and energetic effects remain largely absent from the current literature. This reveals a gap in current research, namely the lack of an integrated framework for assessing lightweight design solutions in hydraulically actuated machinery, considering both dynamic behavior and energy consumption of operation in application.

Addressing this gap requires flexible multibody simulation techniques capable of accurately capturing dynamic structural behavior under realistic operating conditions

(e.g. variable loading scenarios and hydraulic actuation effects). Moreover, to enable early stage evaluations and to support integration with modern engineering practices, including Hardware-in-the-Loop (HIL) testing and real-time capable digital twin applications [13], these simulations must meet real time computational constraints.

Achieving such real-time capable simulation remains a significant challenge. Existing methods, including analytical approaches, assumed mode methods [14], transfer matrix methods [15], finite element (FE) models [11], and classical floating frame of reference formulations (FFRF), often fail to meet the real-time requirements for three-dimensional (3D) flexible systems. Furthermore, coupling flexible structural models with hydraulic actuation adds another layer of computational complexity. Among several FFRF extensions, generalized Component Mode Synthesis (CMS) techniques have proven particularly effective for 3D flexible multibody systems [16–18], and recent studies demonstrate their efficiency even when combined with hydraulic dynamics [19].

The objective of this study is to develop and demonstrate a workflow for the lightweight design of hydraulically actuated machinery, accounting for both structural mass reduction and energy efficiency evaluation. The workflow is demonstrated on a simplified hydraulically actuated mechanism derived from a forestry crane. The main contributions are threefold:

- minimizing structural weight under bending resistance and stability constraints,
- identifying modal characteristics critical for dynamic performance, and
- analyzing the impact of weight reduction on hydraulic energy consumption during operational cycles.

This integrated approach supports the development of lighter, more energy-efficient hydraulic machinery. By incorporating real-time capable flexible simulation, this work advances the development of smart, sustainable mobile machinery and digital twin-based engineering systems.

2 Workflow and model description

A schematic workflow is introduced in Fig. 1 for designing energy-efficient hydraulically actuated flexible multibody systems. It comprises of standard structural optimization process, linear structural analysis and evaluation of energy efficiency through flexible multibody dynamic simulation. Theoretical background of components in workflow is briefly described in the following subsections.

The flexible multibody system depicted in Fig. 1 serves as a demonstrator for our proposed workflow. It consists of a rigid pillar, flexible lift boom and a point mass m and joints. The lift boom is actuated with a double acting hydraulic cylinder, that is connected through 4/3 hydraulic directional control valve to pump and tank.

The lift boom as depicted in Fig. 2 was identified as an ideal subject for structural optimization as it is the most heavily loaded and heaviest component in the entire mechanism. The default lift boom, manufactured with RAEX 640 steel, is redesigned in this study to take advantage of Ultra-High Strength Steel (UHSS) with a higher tensile yield strength. The material properties used in this analysis are given in Table 1.

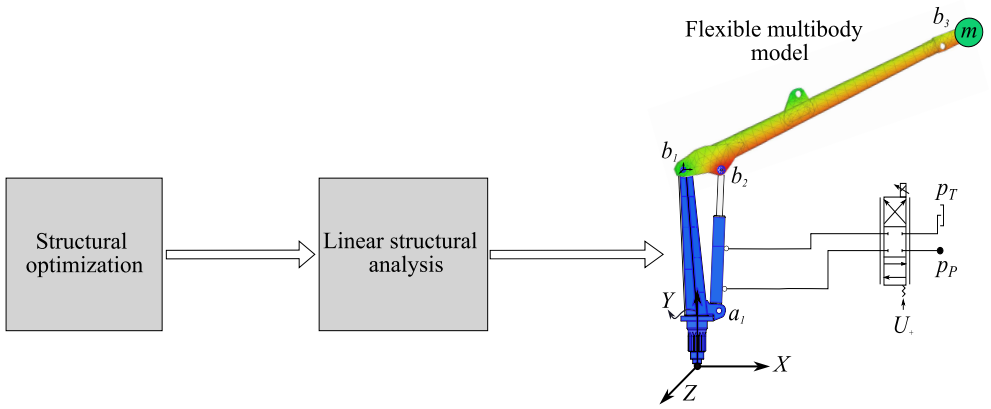


Fig. 1: Schematic workflow for designing energy-efficient machines.

Table 1: Material Properties

Material	**Density** (kg/m^3)	**Young's Modulus** (GPa)	**Tensile Yield Strength** (MPa)	**Poisson's Ratio**
RAEX 640	7850	210	640	0.3
UHSS	7850	210	1100	0.3

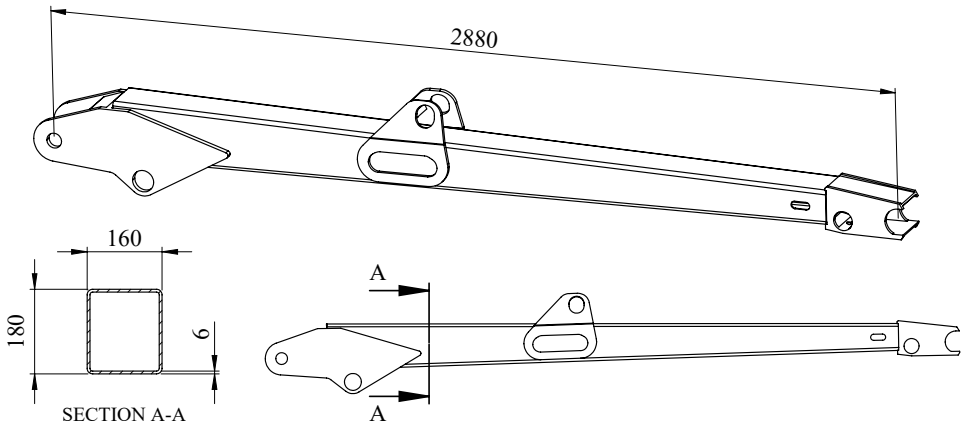


Fig. 2: Default lift boom geometry and cross section dimensions.

2.1 Structural optimization algorithm

Structural optimization typically involves a reduction structural weight while preserving key mechanical characteristics. In steel crane boom structures, the optimization

can be conducted by changing the shape and dimensions of cross section, as well as steel grade. The cross sectional dimensions and material grade are linked: a change in the steel grade affects the optimal plate dimensions (see Eq. 5). In crane boom structures, closed-form cross-sectional shapes are typically applied. The cross section can be thought to be comprised of plate parts that are connected to each other to form a closed shape. This section presents a method to optimize closed-form rectangular hollow section (RHS) beam profile to maintain flexural moment capacity at the major axis. The equations work for other more complex closed profiles when implemented correctly.

The optimization procedure applies the flexural moment capacity in the major axis as a requirement for new profiles. The flexural moment capacity is calculated based on the yield criterion in the uniaxial stress state:

$$M = W_{\mathrm{el}} f_{\mathrm{y}}, \tag{1}$$

where W_{el} is the elastic section modulus and f_{y} is the yield strength of material. The elastic section modulus can be calculated with equation:

$$W_{\mathrm{el}} = \frac{I}{c}, \tag{2}$$

where I is the second moment of area, and c is the maximum distance from neutral axis.

To design a cross-section as per the elastic distribution of stresses with the extreme compression fiber stress equal to the yield strength of material, cross-sectional dimensions of the profile should satisfy the Class 3 requirements [20]. The width of individual parts, i.e., the web and compression flange members of the RHS, is constrained by the buckling capacity, which is analyzed according to [20]. For the bending-loaded crane boom structures with RHS profile with internal elements, the allowable width-to-thickness ratio based on the Class 3 cross section can be determined with functions:

$$\text{when } \psi > -1 : w/t = \frac{38\epsilon}{0.608 + 0.343 + 0.049\psi^2} \tag{3}$$

$$\text{when } \psi \leq -1 : w/t \leq 60.5\epsilon(1 - \psi), \tag{4}$$

where w is the maximum plate dimension. Yield strength-dependent coefficient ϵ is defined as

$$\epsilon = \sqrt{\frac{235}{f_{\mathrm{y}}}} \tag{5}$$

where f_{y} is given in MPa. Stress ratio ψ is defined as

$$\psi = \frac{\sigma_2}{\sigma_1}, \tag{6}$$

where σ_1 is the maximum compressive stress in the part and σ_2 is the stress at the other side of the part. For the bending-loaded RHS cross-section, the stress ratios are $\psi = -1$ (pure bending) and $\psi = 1$ (uniform compression) for the web and compression

flange members, respectively. The maximum allowable part width-to-thickness ratios are calculated with Eq. 3 and 4. To obtain outer width and height of the RHS cross-section produced by cold forming, $3t$ can be added to consider the rounding of the corners.

The optimization can be carried out considering the cross-section at the maximum bending moment location. Default cross section properties, such as the section modulus, can be used as a requirement for comparing the different cross sections. Cross-section properties are calculated with different possible parameter combinations. If the chosen constraints are satisfied, cross-section is saved to possible combinations. In general, not all combinations are desired but values that satisfy the manufacturing requirements. For example the thickness of the profile can be chosen to increase with an incremental step of 1 mm. When all possible combinations within set limits are tested, optimal solutions can be output. Typically the smallest cross-section and thereby the lightest variant is ideal, however other criteria can be applied. The flowchart for the parameter optimization is shown in Fig. 3. Based on the optimized parameters obtained from the algorithm shown in Fig. 3, an optimized lift boom model with the new cross-section dimensions is prepared.

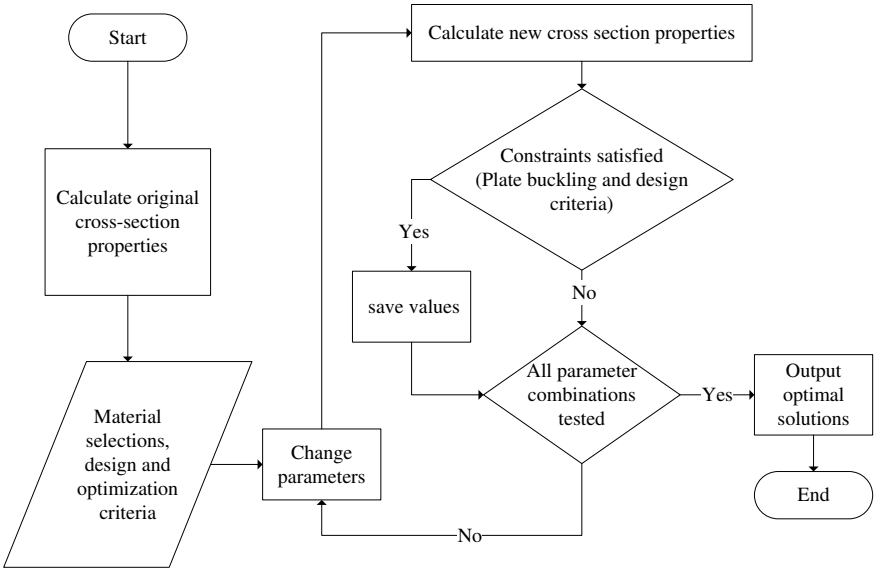


Fig. 3: Cross-section optimization flowchart.

2.2 Linear structural analysis

After creating a CAD model, both the default and optimized lift booms are discretized in finite element (FE) software and subjected to linear structural analysis. In a static structural study, stresses and deformations are calculated for the prescribed loads, with special attention to the area where maximum stresses occur, so that the ultimate moment capacity of the two models can be compared.

In the subsequent eigenfrequency study, natural frequencies and mode shapes of the flexible body are extracted to characterize its dynamic behavior. In eigenfrequency analysis the dynamic equilibrium of a discretised structure can be modeled as [21],

$$\mathbf{M}\,\ddot{\mathbf{u}} + \mathbf{C}\,\dot{\mathbf{u}} + \mathbf{K}\,\mathbf{u} = \mathbf{F}, \tag{7}$$

where $\mathbf{M}$, $\mathbf{C}$ and $\mathbf{K}$ are the global mass matrix, damping matrix and stiffness matrix, $\mathbf{u}$ is the nodal-displacement vector, and $\mathbf{F}(t)$ is the external excitation. Neglecting damping and external forces gives the free-vibration form

$$\mathbf{M}\,\ddot{\mathbf{u}} + \mathbf{K}\,\mathbf{u} = \mathbf{0} \tag{8}$$

Assuming a harmonic response $\mathbf{u} = \phi_i \cos(\omega_i t)$ and inserting it into Eq. (8) yields the classical eigenvalue problem

$$\left(\mathbf{K} - \omega_i^2 \mathbf{M}\right) \boldsymbol{\phi}_i = \mathbf{0} \tag{9}$$

Non-trivial solutions exist only when $\det(\mathbf{K} - \omega_i^2 \mathbf{M}) = 0$, providing the eigenvalues ω_i^2 and mode shapes $\boldsymbol{\phi}_i$. The circular natural frequencies are converted to the ordinarily quoted natural frequencies by

$$f_i = \frac{\omega_i}{2\pi} \tag{10}$$

Eq. (7)–(10) furnish the foundation of eigenfrequency analysis where the eigenpairs $(\omega_i, \boldsymbol{\phi}_i)$ describe how stiffness and mass distribute vibration energy, enabling designers to avoid resonance. Furthermore, the analysis provides nodal coordinates, as well as mass and stiffness matrices, to generate a flexible lift boom for a subsequent multibody dynamics simulations [18].

2.3 Flexible multibody simulation

A hydraulically actuated constrained flexible multibody system can be modeled as [22],

$$\mathbf{M}(\mathbf{q})\ddot{\mathbf{q}} + (\mathbf{G}_\mathbf{q})^\top \boldsymbol{\lambda} = \mathbf{Q}(\mathbf{q}, \dot{\mathbf{q}}, \mathbf{u}, t), \tag{11}$$

$$\mathbf{G}(\mathbf{q}, t) = \mathbf{0}, \quad \text{and} \tag{12}$$

$$\dot{\mathbf{y}} + \frac{\partial \mathbf{G}}{\partial \mathbf{y}^\top} \boldsymbol{\lambda} = \mathbf{f}_{\mathrm{ODE}_1}(\mathbf{q}, \dot{\mathbf{q}}, \mathbf{u}, t), \tag{13}$$

where $\mathbf{q}, \dot{\mathbf{q}}, \ddot{\mathbf{q}} \in \mathbb{R}^n$ are the generalized position, velocity and acceleration vectors in n number of system coordinates, $\mathbf{M} \in \mathbb{R}^{n \times n}$ is system mass matrix, $\mathbf{Q} \in \mathbb{R}^n$ is the

generalized force vector, $\mathbf{G_q}$ is the jacobian of holonomic constraint equations $\mathbf{G}$, $\boldsymbol{\lambda}$ is the vector of Lagrange-multipliers and $\mathbf{u}$ is the control signal. Further details about $\mathbf{M}$ and $\mathbf{Q}$ for the flexible bodies can be found in [18]. The details of these matrices can be exported from standard FE-software following linear structural analysis. For a flexible multibody system, the modeling of joints, $\mathbf{G}$ and $\mathbf{G_q}$ is further described in [23].

A hydraulic actuator is coupled into the flexible body by defining nodes at the connection point and applying standard RBE2 boundary condition [19]. For a hydraulically actuated system, $\mathbf{y}$ in Eq. (13) demonstrates the hydraulic pressure, p_{h_i}. The hydraulic pressure derivative, $\dot{p}_{h_i}$, can be expressed through a hydraulic volume V_{h_i} as,

$$\dot{p}_{h_i} = \frac{B_{e_{h_i}}}{V_{h_i}} \left(-\frac{dV_{h_i}}{dt} + Q_{s_i} \right), \tag{14}$$

$$B_{e_h} = \left(\frac{1}{B_o} + \sum_{c=1}^{n_h} \frac{V_c}{V_h B_c} \right)^{-1} \tag{15}$$

where Q_{s_i} is the flow rate, $B_{e_{h_i}}$ is the effective bulk modulus, B_o is the oil bulk modulus, B_c is the bulk modulus in a sub-volume V_c and n_h is the number of hydraulic volumes. The force F_h produced by a hydraulic actuator can be described as,

$$F_h = p_{h_1} A_{h_1} - p_{h_2} A_{h_2} - F_\mu, \tag{16}$$

where p_{h_1} and p_{h_2} are the pressures in cylinder areas A_{h_1} and A_{h_2}, respectively, and F_μ is the cylinder friction force. The force F_μ in the hydraulic cylinder is computed according to [24].

The mechanical energy transferred from the hydraulic cylinder to the lift boom over the evaluated motion period is given by:

$$E_h = \int_{x_0}^{x_1} F_h(x)\, dx, \tag{17}$$

where x_0 and x_1 denote the initial and final piston extension positions, respectively, and $F_h(x)$ is the hydraulic force as a function of piston displacement. In the simulation, this expression is evaluated numerically as:

$$E_h \approx \sum_i F_{h,i} \cdot \Delta x_i, \tag{18}$$

where $F_{h,i}$ is the hydraulic force at step i, and Δx_i is the incremental piston displacement between steps.

3 Workflow implementation and results

The results follow the workflow proposed in Fig. 1. The results consist of analyzing the structure shown in Fig. 2. Structural optimization results are shown in Section 3.1. Static, eigenvalue and energy efficiency analysis results are shown in Section 3.2, Section 3.3 and Section 3.4 respectively.

3.1 Structural optimization for weight reduction

The optimization algorithm (Fig. 3) was run with two design criteria. The non-prismatic shape was kept similar to the original geometry (height along the length). A modification of the shape requires redesign and optimization of the connected parts, such as the bracket plates welded to the web to which the pins for hydraulic actuators are connected. The second criterion was that the in-plane moment capacity needed to be similar to one of the original geometry. This left two geometric parameters to be considered which were width b and thickness t. The default cross-section dimensions at the location of maximum bending stresses were h = 180 mm, b = 160 mm and t = 6 mm. After conducting the optimization algorithm, two alternative cross sections with different thickness were obtained, see Table 2.

The cross section, resulting in the smallest area (Case 1), was chosen as the optimized version. Its width is narrower than in the original boom, which might cause stability problems if out-of-plane motion occurs. As stated earlier, that was not considered in the current analysis. After the optimization process, a new CAD model with new cross-sectional dimensions was created as depicted in Fig. 4. Mass of the default model with the connected parts shown in Fig. 2 was 121 kg and mass of the optimized model shown in Fig. 4 was 94.5 kg. Total weight reduction of the structure was 21.9 %.

Table 2: Cross-section values of original and two different options

Version	h [mm]	b [mm]	t [mm]	W_x [mm^3]	A [mm^2]	**Area reduction** [%]	M_x [kNm]
Original	180	160	6	214 221	3 936	–	137.1
1	180	95	5	126 329	2 650	32.7	139.0
2	180	75	6	133 452	2 976	25.9	141.8

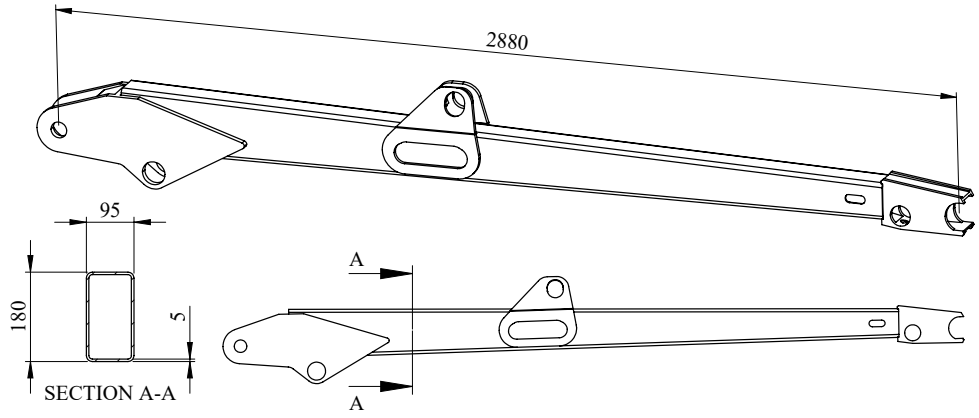


Fig. 4: Optimized boom geometry and cross-section dimensions.

3.2 Static analysis

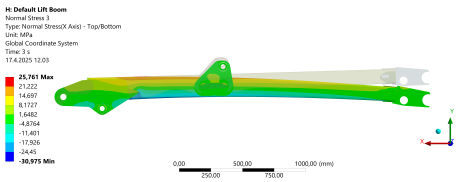
After discretization of three-dimensional CAD model of both lift boom models, linear static FE-analysis was performed in the commercial FE-ANSYS software. The boom was modeled with plate elements (SHELL181) and cylinder brackets with solid elements (SOLID186). Mesh sizes of 10 mm and 30 mm were used for the shell and solid elements, respectively. Total number of shell elements was 23 584 and total number of solid elements was 840 in the default model. The shell elements were connected to the solid elements via bonded contacts using ANSYS default settings.

The boundary conditions applied in the linear static analysis are illustrated in Fig. 1. Boundary condition b_1 represents the pillar-lift boom connection point, was modeled as a revolute joint, constraining all translational degrees of freedom as well as rotational motion about the X- and Y-axes, but allowing rotation about Z-axis. The second boundary condition was set as general joint in the hydraulic cylinder-lift boom attachment point b_2. Translation was restricted in the Y-axis of the local coordinate system, aligned with the axis of the cylinder.

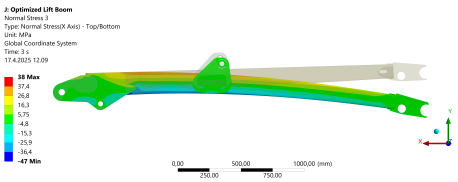
Load b_3 chosen was a 200 kg mass at the boom tip, which was set to the model as a vertical force along the negative Y-axis in the global coordinate system. The analyses were carried out without modeling gravity, since gravity was excluded in the analytical calculations, and stress analysis results were validated with the analytical calculations.

Fig. 5 shows a comparison of static structural analysis for default and optimized lift booms under the boundary conditions. The bending stress of the default lift boom was 21.5 MPa and 37.5 MPa in the optimized lift boom as shown in Fig. 5a and Fig. 5b respectively.

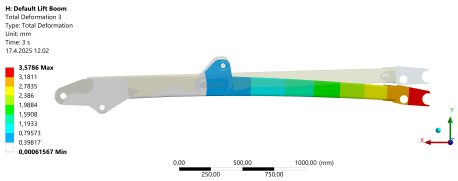
As demonstrated in Fig. 5c and Fig. 5d , the total deformation of the default lift boom was 3.57 mm and the total deformation of the optimized lift boom with UHSS is 5.99 mm. The deformation in the optimized lift boom was higher than that of in the default lift boom model. The Von Mises stresses in the default and optimized lift



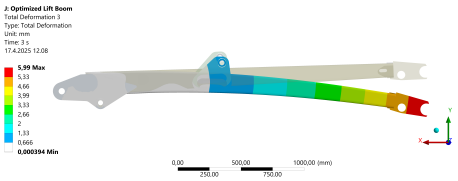
(a) Bending stress σ_x of default model.



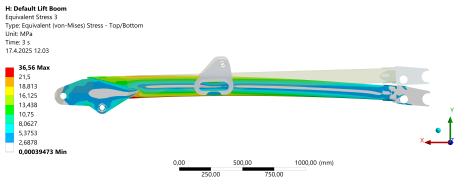
(b) Bending stress σ_x of optimized model.



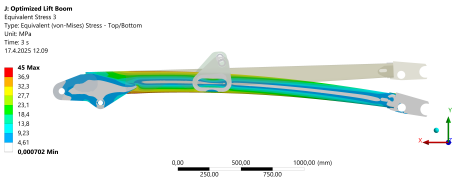
(c) Deformation δ of default model.



(d) Deformation δ of optimized model.



(e) Von Mises stress of default model.



(f) Von Mises stress of optimized model.

Fig. 5: **Static analysis:** Comparing the bending stress, deformation and Von Mises stresses of default model and optimized lift boom.

booms were 21.7 MPa and 37.1 MPa, as also shown in Fig. 5e and Fig. 5f respectively. Both the maximum equivalent stress and normal stress of the optimized model were higher than the default. A comparison of the normal stress, analytical calculation of bending stress and deformation values are presented in Table 3.

Table 3: Stress and deformation results of the default and the optimized versions

	Normal stress σ_x at top flange (MPa)	**Analytical bending stress** (MPa)	**Deformation** (mm)
Default	21.5	19.4	3.58
Optimized	37.5	34.9	5.99

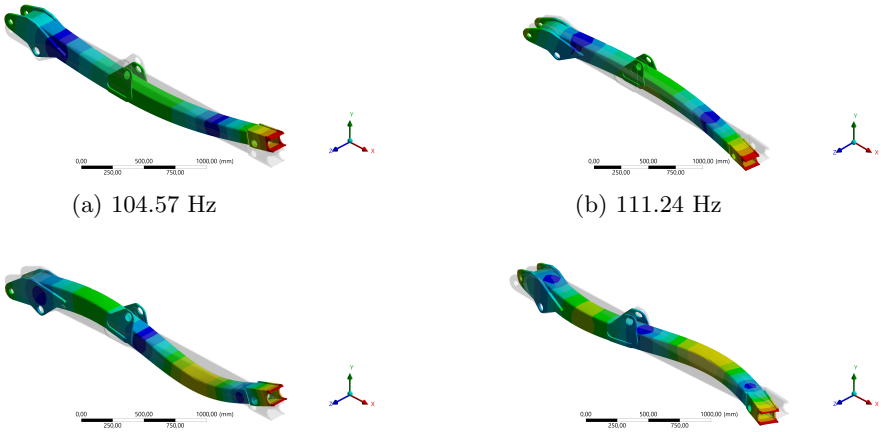
3.3 Eigenfrequency analysis

For dynamic performance, the eigenfrequency analysis was performed on default and optimized lift boom structures. To reduce the complexity of the analysis, the CAD model of lift booms were converted into a single solid body. This ensured mesh continuity and allowed accurate generation of reduced-order models. Because no displacement constraints were imposed, the analysis reveals the both boom's inherent dynamic behavior. So, the first six modes were rigid body motions that are numerically very close to 0 Hz from orders 1-6 as shown in Table 4 for both lift boom variants. Table 4 listed the first ten natural frequencies and their dominant shapes, while Fig. 6 and Fig. 7 visualize the bending modes that govern the dynamic response.

Table 4: Natural frequencies and mode shapes for the both lift boom variants.

Order	**Default lift boom**		**Optimized lift boom**	
	f_n [Hz]	**Mode description**	f_n [Hz]	**Mode description**
1	0	Rigid motion	0	Rigid motion
2	0		0	
3	0		6.78×10^{-4}	
4	7.91×10^{-4}		1.59×10^{-3}	
5	1.74×10^{-3}		2.08×10^{-3}	
6	2.11×10^{-3}		5.74×10^{-3}	
7	104.57	1st bending, Y-direction (Fig. 6a)	67.52	1st bending, X-direction (Fig. 7a)
8	111.24	1st bending, X-direction (Fig. 6b)	92.17	1st bending, Y-direction (Fig. 7b)
9	298.94	2nd bending, Y-direction (Fig. 6c)	194.53	2nd bending, X-direction (Fig. 7c)
10	313.23	2nd bending, X-direction (Fig. 6d)	270.45	2nd bending, Y-direction (Fig. 7d)

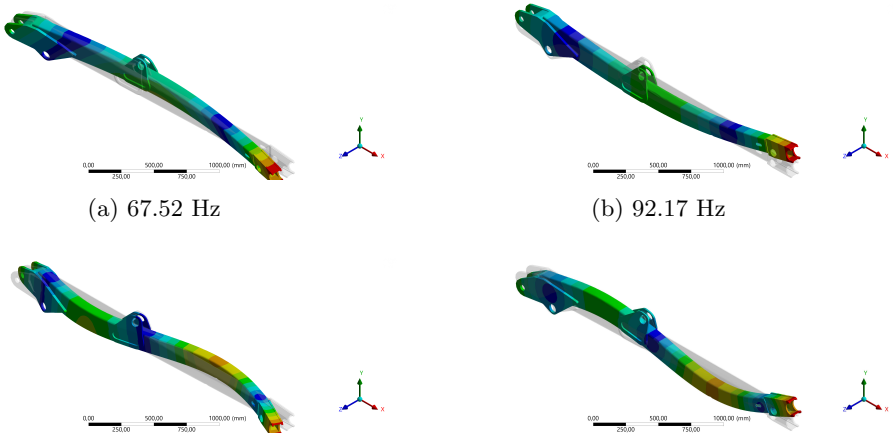
As seen in Table 4, in the optimized lift boom, the first bending mode in the horizontal direction is reduced from 111.24 Hz (Fig. 6b) to 67.52 Hz (Fig. 7a) resulting in a 43.72 Hz (39.3%) reduction with respect to the default lift boom. Compared to the width of the default boom, which is 160 mm, and the optimized boom at 95 mm, making it 65 mm (40.63%) narrower than the default lift boom and thereby dominates the dynamic performance. The vertical direction first bending mode drops from 104.57 Hz to 92.17 Hz, which is 88.14% of the original structure's first vertical bending mode frequency. In the geometry, the height has been same in both structures, and the only difference is the reduction of wall thickness from 6 mm to 5 mm making it 83.33% from the original wall thickness. Typically, the first bending mode is the most prominent, and thereby focused in the results evaluation.



(a) 104.57 Hz (b) 111.24 Hz

(c) 298.94 Hz (d) 313.23 Hz

Fig. 6: **Default lift boom:** Flexible bending eigenmodes (orders 7–10).



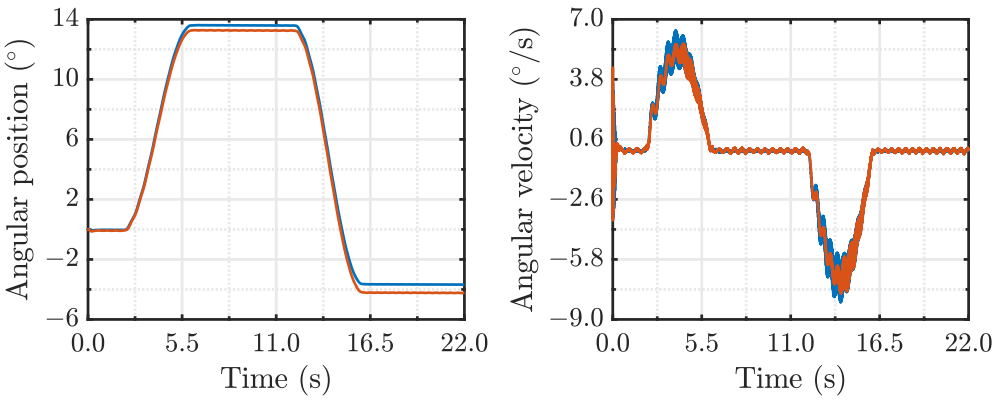
(a) 67.52 Hz (b) 92.17 Hz

(c) 194.53 Hz (d) 270.45 Hz

Fig. 7: **Optimized lift boom:** Flexible bending eigenmodes (orders 7–10).

3.4 Energy efficiency analysis

Fig. 8 and Fig. 9 present comparison of both lift boom variants under an identical proportional valve input signal during the extension (0–8 seconds) and retraction (10–18 seconds) phases of a hydraulic cylinder. The input signal was modeled using spline functions, and the motion trajectory was not actively controlled. Hydraulic cylinder friction and joint friction were not considered in this analysis.



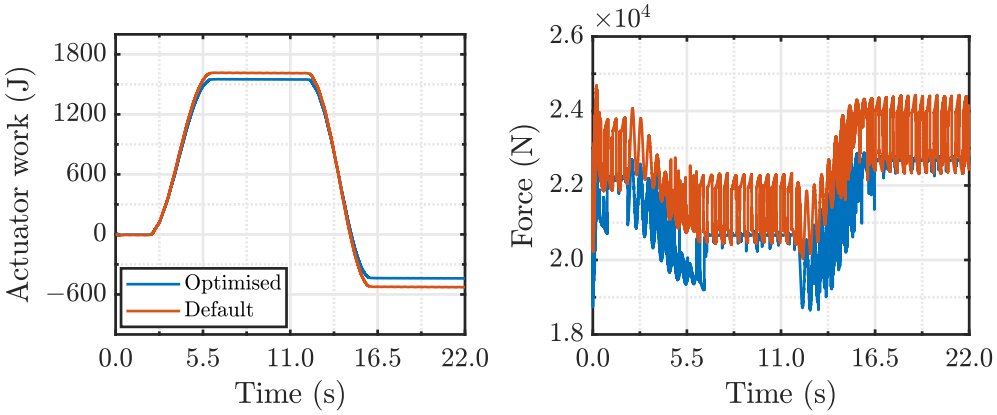
(a) Angular position of lift boom.

(b) Angular velocity of lift boom.

Fig. 8: Comparison of working cycle for both lift boom variants under identical proportional valve input.

As shown in Fig. 8a and 8b, during the extension phase, the optimized lift boom achieved a 2.5% higher angular position and a slightly higher angular velocity while requiring 4% less mechanical work compared to the default variant, as illustrated in Fig. 9a. During retraction, the additional mass provided gravitational assistance, reducing the relative mechanical work of the optimized lift boom by 7% and achieving a 1.3% lower angular position compared to the default boom. Notably, in both cases, the motion stopped below the initial angular position.

Fig. 9b shows fluctuating actuator forces throughout both motion phases, with a prominent peak at the beginning of the simulation, attributed to improper static initialization of the simulation model.



(a) Hydraulic actuator work.

(b) Hydraulic actuator force.

Fig. 9: Comparison of actuator work and force of both lift boom variants under identical proportional valve input.

4 Discussion and Conclusion

This study presents a workflow aimed at enhancing energy efficiency in hydraulically actuated machinery, achieved through the optimization of a flexible lift boom. The default boom structure, made of RAEX 640 steel, was structurally optimized toward a weight reduction using UHSS. The structural optimization algorithm was applied to the default lift boom, focusing on weight reduction while preserving the equivalent in-plane moment capacity. The default and optimized lift boom variants were subsequently meshed for linear structural analysis to evaluate its static and dynamic characteristics. The results of these analyses generated the required matrices for development a flexible multibody simulation model. This enabled further evaluation of energy efficiency of the system in real time simulation environment.

The study yielded the following key findings:

- The implementation of UHSS in place of the default material led to a 32.7% reduction in cross-sectional area and a 21.9% reduction in weight (excluding accessories).
- Linear static analysis revealed a 67% increase in tip deflection. Eigenfrequency analysis indicated that the first bending mode shifted from 104.6 Hz (vertical plane) to 67.5 Hz (horizontal plane), identifying a new horizontal-plane critical mode due to the narrower geometry.
- Flexible multibody simulation revealed that during the extension phase, the optimized lift boom achieved a 2.5% higher angular position while requiring 4% less mechanical work. During retraction, the relative mechanical work of the optimized lift boom variant was 7% lower and resulted in a 1.3% lower angular position compared to the default boom.

These results are consistent with existing literature [8], [9], which highlights the trade-offs inherent in lightweight design strategies. Moreover, the credibility of energy efficiency estimations is highly dependent on the accuracy of both the flexible multibody simulation model and the hydraulic system representation. While the workflow showed potential for improving energy efficiency, it was not explicitly considered as an optimization objective. Notably, fatigue strength criterion and out-of -plane load effects were not addressed in the current workflow.

Addressing the fatigue strength criterion would require the extraction of stress-time histories from the real-time capable flexible multibody simulation and the integration of an additional design loop based on fatigue-life criteria into the workflow. This represents a significant technical challenge. Although real-time capable flexible multibody simulation is not strictly necessary for fatigue analysis, it is justified by the intention to integrate the workflow with HIL testing and to support the development of real-time capable digital twin applications in machinery. Consequently, this research not only addresses current challenges in lightweight design for hydraulically actuated systems but also establishes a foundation for real-time digital twin development, supporting the evolution of smart, energy-efficient heavy machinery.

Future research will expand the optimization framework by incorporating both in-plane and out-of-plane load conditions, with a focus on improving structural performance and fatigue. The design space will be broadened by varying boom geometry and adapting associated components accordingly. Fatigue strength assessment will be integrated using stress-time histories extracted from real-time capable flexible multibody simulations. For example, recent advances in deep neural networks offer promising potential for structural optimization and real-time stress extraction.

5 Statements and Declarations

All authors certify that they have no affiliations with or involvement in any organization or entity with any financial interest or non-financial interest in the subject matter or materials discussed in this manuscript.

6 Acknowledgements

The authors are grateful for financial support from Business Finland for the funding in the Virtual Material Engineering (VIIMA) project (Grant ID: 6153/31/2023).

References

[1] Lindgren, M.: A Transient Fuel Consumption Model for Non-road Mobile Machinery. Biosystems Engineering **91**, 139–147 (2005) https://doi.org/10.1016/j.biosystemseng.2005.03.011

[2] Söderena, P., Pihlatie, M., Nylund, N.-O.: Pathways for CO2 Regulation in NRMM. VTT Research Report, vol. VTT-CR-0032-24. VTT Technical Research Centre of Finland, Finland (2024). VTT-CR-0032-24

[3] Czerwinski, F.: Current trends in automotive lightweighting strategies and materials. Materials **14**(21), 6631 (2021) https://doi.org/10.3390/ma14216631

[4] Lajunen, A., Sainio, P., Laurila, L., Pippuri-Mäkeläinen, J., Tammi, K.: Overview of powertrain electrification and future scenarios for non-road mobile machinery. Energies **11**(5), 1184 (2018) https://doi.org/10.3390/en11051184

[5] Herrmann, C., Dewulf, W., Hauschild, M., Kaluza, A., Kara, S., Skerlos, S.: Life cycle engineering of lightweight structures. Cirp Annals **67**(2), 651–672 (2018) https://doi.org/10.1016/j.cirp.2018.05.005

[6] Gufler, V., Wehrle, E., Zwölfer, A.: A review of flexible multibody dynamics for gradient-based design optimization. Multibody System Dynamics **53**(4), 379–409 (2021) https://doi.org/10.1007/s11044-021-09802-z

[7] Ashby, M.F.: Materials Selection in Mechanical Design. Butterworth-Heinemann, Oxford (2011). https://doi.org/10.1016/B978-1-85617-663-7.00002-3

[8] Zhang, H., Ge, X.-b., Li, Y., Shao, X.-d., Jia, M.-m.: Lightweight design of excavator working device based on automatically generated surrogate model. Scientific Reports **14**, 29756 (2024) https://doi.org/10.1038/s41598-024-80882-5

[9] Solazzi, L., Assi, A., Ceresoli, F.: Excavator arms: Numerical, experimental and new concept design. Composite Structures **217**, 60–74 (2019) https://doi.org/10.1016/j.compstruct.2019.02.096

[10] Sarkhel, P., Dikshit, M.K., Pathak, V.K., Saxena, K.K., Prakash, C., Buddhi, D.: Robust deflection control and analysis of a fishing rod-type flexible robotic manipulator for collaborative robotics. Robotics and Autonomous Systems **159**, 104293 (2023) https://doi.org/10.1016/j.robot.2022.104293

[11] Uyar, M., Malgaca, L.: Implementation of active and passive vibration control of flexible smart composite manipulators with genetic algorithm. Arabian Journal for Science and Engineering **48**(3), 3843–3862 (2023)

[12] Rigatos, G., Busawon, K.: Robotic Manipulators and Vehicles: Control, Estimation and Filtering. Studies in Systems, Decision and Control, vol. 152. Springer, Cham (2018)

[13] Kurvinen, E., Kutvonen, A., Ukko, J., Khadim, Q., Hagh, Y.S., Jaiswal, S., Neisi, N., Zhidchenko, V., Kortelainen, J., Timperi, M., *et al.*: Physics-based digital twins merging with machines: Cases of mobile log crane and rotating machine. IEEE Access **10**, 45962–45978 (2022) https://doi.org/10.1109/ACCESS.2022.3170430

[14] Sun, C., Gao, H., He, W., Yu, Y.: Fuzzy neural network control of a flexible robotic manipulator using assumed mode method. IEEE Transactions on Neural

Networks and Learning Systems **29**(11), 5214–5227 (2018) https://doi.org/10.1109/TNNLS.2017.2743103

[15] Shi, M., Rong, B., Liang, J., Zhao, W., Pan, H.: Dynamics analysis and vibration suppression of a spatial rigid-flexible link manipulator based on transfer matrix method of multibody system. Nonlinear Dynamics **111**(2), 1139–1159 (2023) https://doi.org/10.1007/s11071-022-07921-6

[16] Zwölfer, A., Gerstmayr, J.: A concise nodal-based derivation of the floating frame of reference formulation for displacement-based solid finite elements: Avoiding inertia shape integrals. Multibody System Dynamics **49**(3), 291–313 (2020) https://doi.org/10.1007/s11044-019-09716-x

[17] Zwölfer, A., Gerstmayr, J.: Co-rotational formulations for 3D flexible multibody systems: a nodal-based approach. Contributions to Advanced Dynamics and Continuum Mechanics, 243–263 (2019) https://doi.org/10.1007/978-3-030-21251-3_14

[18] Zwölfer, A., Gerstmayr, J.: The nodal-based floating frame of reference formulation with modal reduction: How to calculate the invariants without a lumped mass approximation. Acta Mechanica **232**, 835–851 (2021) https://doi.org/10.1007/s00707-020-02886-2

[19] Khadim, Q., Manzl, P., Kurvinen, E., Mikkola, A., Orzechowski, G., Gerstmayr, J.: Real-time structural deflection estimation in hydraulically actuated systems using 3D flexible multibody simulation and dnns. arXiv preprint arXiv:2503.07528 (2025)

[20] Eurocode 3. Design of steel structures. Part 1-1: General rules and rules for buildings. Standard, European Committee for Standardization (November 2022)

[21] Xiao, C., Guiju, Z.: Modal analysis on working equipment of hydraulic excavator. The Open Mechanical Engineering Journal **9**(1), 173–180 (2015)

[22] Gerstmayr, J.: Exudyn– A C++ based Python package for flexible multibody systems. Multibody System Dynamics **60**(4), 533–561 (2023) https://doi.org/10.1007/s11044-023-09937-1

[23] Gerstmayr, J., Holzinger, S., Zwölfer, A.: From 3D solid finite elements to reduced flexible multibody bodies with constraint interfaces: A holistic approach. Journal of Sound and Vibration **Under Review** (2025)

[24] Brown, P., McPhee, J.: A continuous velocity-based friction model for dynamics and control with physically meaningful parameters. Journal of Computational and Nonlinear Dynamics **11**(5), 054502 (2016) https://doi.org/10.1115/1.4033658